XL CILAMCE
IBERO-LATIN AMERICAN CONGRESS ON COMPUTATIONAL METHODS IN ENGINEERING
NOVEMBER 11-14, 2019
Praiamar Natal Hotel & Convention Natal, RN-BRAZIL

EVALUATION OF EFFECTIVE THERMOELASTIC PROPERTIES OF PERIODIC COMPOSITES USING A THREE-DIMENSIONAL FINITE-VOLUME MODEL

Camila S. Vieira
milavieira@gmail.com
Federal University of Sergipe
CCET, Avenida Marechal Rondon, s/n, 49100-000, São Cristovão – SE.
Severino P. C. Marques
smarques@ctec.ufal.br
Federal University of Alagoas
Center of Technology, Campus A. C. Simões, 57072-900, Maceió, Alagoas, Brazil

Abstract. The prediction of the effective thermomechanical behavior of composite materials has been a matter of great interest over the last decades. This is justified because in many important industrial applications such materials are subjected simultaneously to high thermal gradients and mechanical loading. The level and distribution of the stress and strain produced by these actions are strongly dependent on the microstructural details of the composite. This work presents a theoretical study on the evaluation of the effective thermoelastic properties of composites with periodic microstructures. The focused effective properties are the elastic moduli and thermal expansion coefficients. For this end, it is applied a three-dimensional micromechanical model based on the parametric finite-volume formulation. In the employed three-dimensional model, the repeating unit cell of the composite is discretized into hexahedral subvolumes to capture the in situ microstructural details. The effective thermal expansion coefficients are evaluated using the well-known Levin's formula. To demonstrate the efficiency of the homogenization model, numerical examples of periodic composites reinforced by short and long aligned fibers are presented and their results are compared with analytical and finite-element solutions.

Keywords: Periodic composites, Effective thermoelastic properties, Three-dimensional model, Finite-volume theory

1 Introduction

Composites are multifunctional materials with a great variety of technological applications in different areas of the science and engineering, extending from micro or nanoelectronic devices to heavy structural systems. Their applications include many situations in which such materials are subjected to large thermal gradients that, together with mechanical loads, can produce critical stress and strain fields. Then, the accurate evaluation of the effective thermoelastic moduli of composites is an important task for their rational applications, as well as for the development of new heterogeneous materials to be used in those thermomechanical environments. Such effective properties include the thermal conductivity, specific heat capacity, coefficients of thermal expansion and elastic moduli.

In the last decades, a great number of analytical and numerical models have been proposed to describe the effective thermoelastic behavior of composites [1,2]. Many of these analytical models are based on the mean-field micromechanics [1,3], originally formulated for elastic homogenization of two-phase composites with random microstructures satisfying the statistical homogeneity condition. Self-consistent model [4], Mori-Tanaka model [5,6], differential scheme [7,8] and double-inclusion method [1] are examples of traditional mean-field micromechanical approaches. The major difference in the formulation of these elastic homogenization procedures consists in the strategy used to take into account the interactions between the phase constituents. The basic idea of the elastic mean-field models has been extended to thermal homogenization problems [9,10].

There is also a lot of micromechanical models proposed to describe the effective thermoelastic behavior of composites with periodic microstructures. Most of these models are based on the concept of repeating unit cell (RUC) as the fundamental building block of the material periodic microstructure. For this class of composites, the numerical homogenization techniques deserve to be highlighted. Finite-element method and finite-volume theory are examples of numerical tools used in the formulation of micromechanical models for periodic composites [2,11-14]. Analytical and semi-analytical approaches based on the equivalent inclusion problem and express in terms of Fourier series are also proposed for homogenization of periodic composites [1,15,16].

This work presents a study on thermoelastic homogenization of composite materials with periodic microstructures. The focused effective properties consist in the elastic moduli and thermal expansion coefficients. For obtaining these overall quantities, a three-dimensional finite-volume model [17,18,19] is employed in conjunction with the well-known Levin's formula for evaluation of the effective thermal expansion coefficients [20]. For the homogenization approach, the repeating unit cell of the composite is discretized into hexahedral subvolumes to capture the in situ microstructural details. To demonstrate the efficiency of the homogenization model, numerical examples of periodic composites reinforced by short and long aligned fibers are presented and their results are compared with analytical and finite-element solutions. The comparisons show a very good performance of the presented numerical procedure.

2 Preliminary considerations

Figure 1 shows a representative volume element (RVE) of a composite material, with volume V and boundary surface S, subjected to a homogeneous displacement boundary condition given by

$$u^0 = \bar{\varepsilon}_{ij} x_j \tag{1}$$

where $\bar{\varepsilon}_{ij}$ $(i, j = 1,2,3)$ are constant strain components and x_j indicate Cartesian coordinates of the points $x \in S$. The displacement field on a repeating unit cell (RUC) of the RVE can be expressed in a two-scale representation as

$$u_i(\boldsymbol{y}') = \bar{\varepsilon}_{ij} x_j + \tilde{u}_i(\boldsymbol{y}') \tag{2}$$

being $\tilde{u}_i(\boldsymbol{y}')$ the fluctuating displacement components on the RUC and $\boldsymbol{y}'$ is the local coordinate vector (Fig. 1).

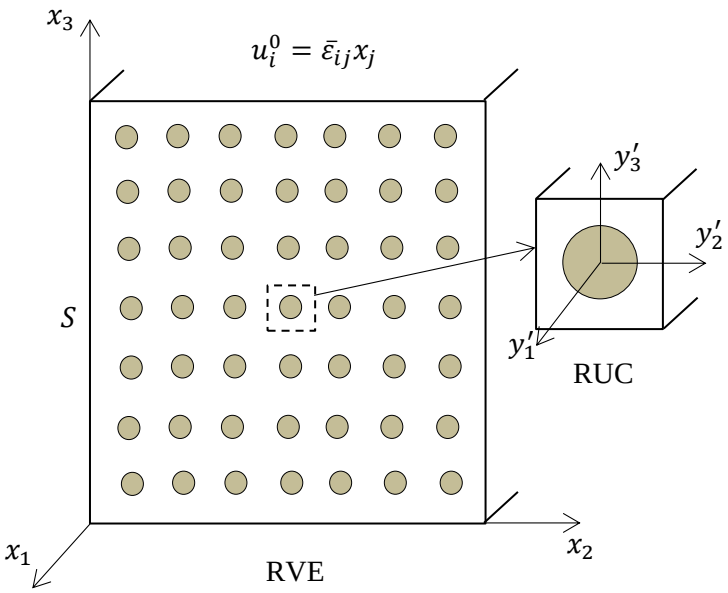

Figure 1. Periodic composite material and repeating unit cell (RUC)

3 Three-dimensional parametric FVDAM for periodic composites

3.1 Outline of the cell unit problem

In the three-dimensional version of the parametric finite-volume theory, the repeating unit cell is discretized into hexahedral subvolumes defined by the locations of their eight vertices expressed in terms of local coordinates y_i $(i = 1,2,3)$, as illustrated in Fig. 2(b) [18,19]. The formulation is based on a mapping of a reference cubic subvolume in the (ζ, η, ξ) parametric space onto each hexahedral subvolume in the (y_1, y_2, y_3) space of the actual repeating unit cell domain (Fig. 2). The reference cubic subvolume is bounded by $-1 \leq \zeta \leq +1$, $-1 \leq \eta \leq +1$ and $-1 \leq \xi \leq +1$.

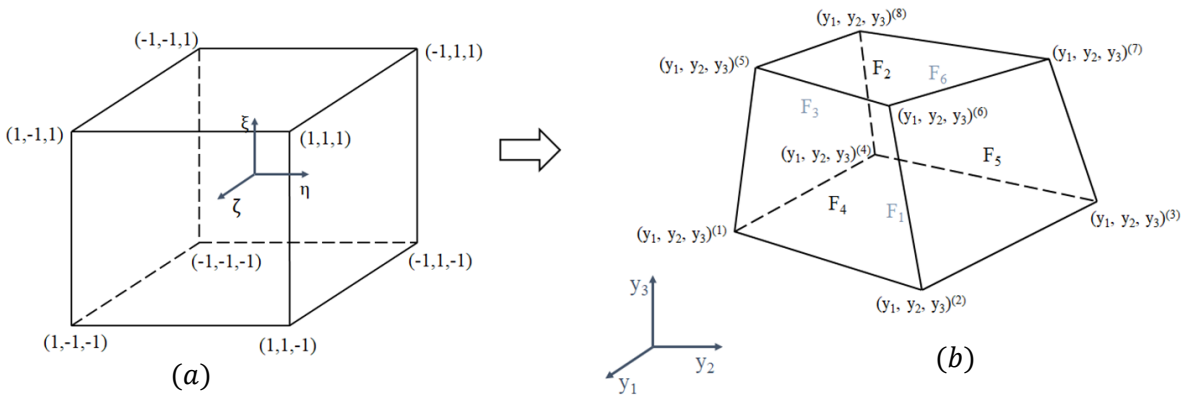

Figure 2. Mapping of the reference cubic subvolume (a) onto the actual hexahedral subvolume (b).

The mapping of a point (ζ, η, ξ) in the reference cubic subvolume to the corresponding point (y_1, y_2, y_3) in the hexahedral subvolume of the repeating unit cell domain is set by the relation [18]

$$y_i(\zeta, \eta, \xi) = \sum_{j=1}^{8} N_j(\zeta, \eta, \xi) y_i^{(j)} \tag{3}$$

where $y_i^{(j)}$ are the coordinates of the *j*-th nodal point of the hexahedral subvolume (Fig. 3b) and

$$N_1(\zeta,\eta,\xi)=\frac{1}{8}(1+\zeta)(1-\eta)(1-\xi) \qquad N_2(\zeta,\eta,\xi)=\frac{1}{8}(1+\zeta)(1+\eta)(1-\xi)$$
$$N_3(\zeta,\eta,\xi)=\frac{1}{8}(1-\zeta)(1+\eta)(1-\xi) \qquad N_4(\zeta,\eta,\xi)=\frac{1}{8}(1-\zeta)(1-\eta)(1-\xi)$$
$$N_5(\zeta,\eta,\xi)=\frac{1}{8}(1+\zeta)(1-\eta)(1+\xi) \qquad N_6(\zeta,\eta,\xi)=\frac{1}{8}(1+\zeta)(1+\eta)(1+\xi)$$
$$N_7(\zeta,\eta,\xi)=\frac{1}{8}(1-\zeta)(1+\eta)(1+\xi) \qquad N_8(\zeta,\eta,\xi)=\frac{1}{8}(1-\zeta)(1-\eta)(1+\xi) \tag{4}$$

For the homogenization approach, the fluctuating displacement field of a subvolume k is approximated by the polynomial expansion

$$\tilde{u}_i^{(k)}=W_{i(000)}^{(k)}+\zeta W_{i(100)}^{(k)}+\eta W_{i(010)}^{(k)}+\xi W_{i(001)}^{(k)}+\frac{1}{2}(3\zeta^2-1)W_{i(200)}^{(k)}+\frac{1}{2}(3\eta^2-1)W_{i(020)}^{(k)}+\frac{1}{2}(3\xi^2-1)W_{i(002)}^{(k)} \tag{5}$$

where $W_{i(mnp)}^{(k)}$ are unknown coefficients to be determined. The equilibrium equations of the subvolume k can be written as

$$\frac{\partial \sigma_{ij}^{(k)}}{\partial y_j}=0 \tag{6}$$

Assuming the material as linear elastic and subjected to a uniform temperature change ΔT, the stress components $\sigma_{ij}^{(k)}$ are related to the strain components $\varepsilon_{ij}^{(k)}$ by the Duhamel-Newmann thermoelastic constitutive relation

$$\sigma_{ij}^{(k)}=C_{ijkl}^{(k)}\varepsilon_{kl}^{(k)}-\sigma_{ij}^{\mathrm{th}(k)} \tag{7}$$

with

$$\sigma_{ij}^{\mathrm{th}(k)}=C_{ijkl}^{(k)}\alpha_{kl}^{(k)}\Delta T\equiv \Gamma_{ij}^{(k)}\Delta T \tag{8}$$

being $C_{ijkl}^{(k)}$ and $\alpha_{kl}^{(k)}$ the elastic stiffness constants and thermal expansion coefficients of the material, respectively. Here, $\Gamma_{ij}^{(k)}=C_{ijkl}^{(k)}\alpha_{kl}^{(k)}$.

Through Eq. (2), the following relation between the strain components and fluctuating displacements is obtained:

$$\varepsilon_{ij}^{(k)}=\bar{\varepsilon}_{ij}+\frac{1}{2}\left(\frac{\partial \tilde{u}_i^{(k)}}{\partial y_j}+\frac{\partial \tilde{u}_j^{(k)}}{\partial y_i}\right) \tag{9}$$

By the parametric finite-volume theory, the first partial derivatives of the fluctuating displacements $\tilde{u}_i^{(k)}$with respect to the parametric (ζ,η,ξ) and Cartesian coordinates $(y_1,y_{2,}y_3)$ are related in the form

$$\begin{Bmatrix} \dfrac{\partial \tilde{u}_i^{(k)}}{\partial y_1} \\ \dfrac{\partial \tilde{u}_i^{(k)}}{\partial y_2} \\ \dfrac{\partial \tilde{u}_i^{(k)}}{\partial y_3} \end{Bmatrix} = \bar{\boldsymbol{J}} \begin{Bmatrix} \dfrac{\partial \tilde{u}_i^{(k)}}{\partial \zeta} \\ \dfrac{\partial \tilde{u}_i^{(k)}}{\partial \eta} \\ \dfrac{\partial \tilde{u}_i^{(k)}}{\partial \xi} \end{Bmatrix} \tag{10}$$

being $\bar{\boldsymbol{J}}$ the inverse of the volume-averaged Jacobian matrix defined by

$$\bar{\boldsymbol{J}} = \frac{1}{8} \int_{-1}^{1} \int_{-1}^{1} \int_{-1}^{1} \boldsymbol{J} d\zeta d\eta d\xi = \begin{bmatrix} A_1 & A_2 & A_3 \\ A_4 & A_5 & A_6 \\ A_7 & A_8 & A_9 \end{bmatrix} \tag{11}$$

where

$$\boldsymbol{J} = \begin{bmatrix} \dfrac{\partial y_1}{\partial \zeta} & \dfrac{\partial y_2}{\partial \zeta} & \dfrac{\partial y_3}{\partial \zeta} \\ \dfrac{\partial y_1}{\partial \eta} & \dfrac{\partial y_2}{\partial \eta} & \dfrac{\partial y_3}{\partial \eta} \\ \dfrac{\partial y_1}{\partial \xi} & \dfrac{\partial y_2}{\partial \xi} & \dfrac{\partial y_3}{\partial \xi} \end{bmatrix} \tag{12}$$

and

$$\begin{aligned}
A_1 &= \frac{1}{8}\left(y_1^{(1)} + y_1^{(2)} - y_1^{(3)} - y_1^{(4)} + y_1^{(5)} + y_1^{(6)} - y_1^{(7)} - y_1^{(8)}\right) \\
A_2 &= \frac{1}{8}\left(y_2^{(1)} + y_2^{(2)} - y_2^{(3)} - y_2^{(4)} + y_2^{(5)} + y_2^{(6)} - y_2^{(7)} - y_2^{(8)}\right) \\
A_3 &= \frac{1}{8}\left(y_3^{(1)} + y_3^{(2)} - y_3^{(3)} - y_3^{(4)} + y_3^{(5)} + y_3^{(6)} - y_3^{(7)} - y_3^{(8)}\right) \\
A_4 &= \frac{1}{8}\left(-y_1^{(1)} + y_1^{(2)} + y_1^{(3)} - y_1^{(4)} - y_1^{(5)} + y_1^{(6)} + y_1^{(7)} - y_1^{(8)}\right) \\
A_5 &= \frac{1}{8}\left(-y_2^{(1)} + y_2^{(2)} + y_2^{(3)} - y_2^{(4)} - y_2^{(5)} + y_2^{(6)} + y_2^{(7)} - y_2^{(8)}\right) \\
A_6 &= \frac{1}{8}\left(-y_3^{(1)} + y_3^{(2)} + y_3^{(3)} - y_3^{(4)} - y_3^{(5)} + y_3^{(6)} + y_3^{(7)} - y_3^{(8)}\right) \\
A_7 &= \frac{1}{8}\left(-y_1^{(1)} - y_1^{(2)} - y_1^{(3)} - y_1^{(4)} + y_1^{(5)} + y_1^{(6)} + y_1^{(7)} + y_1^{(8)}\right) \\
A_8 &= \frac{1}{8}\left(-y_2^{(1)} - y_2^{(2)} - y_2^{(3)} - y_2^{(4)} + y_2^{(5)} + y_2^{(6)} + y_2^{(7)} + y_2^{(8)}\right) \\
A_9 &= \frac{1}{8}\left(-y_3^{(1)} - y_3^{(2)} - y_3^{(3)} - y_3^{(4)} + y_3^{(5)} + y_3^{(6)} + y_3^{(7)} + y_3^{(8)}\right)
\end{aligned} \tag{13}$$

In the next section the superscript representing the subvolume number will be omitting.

3.2 Stiffness matrix of a subvolume

Considering the polynomial expansion (5), the surface-averaged displacements on the subvolume faces (Fig. 2b) are defined by

$$\langle\tilde{u}_i\rangle^{(1,2)} = \frac{1}{4}\int_{-1}^{1}\int_{-1}^{1}\tilde{u}_i(\zeta,\eta,\xi=\mp1)d\zeta d\eta = W_{i(000)} \mp W_{i(001)} + W_{i(002)}$$

$$\langle\tilde{u}_i\rangle^{(3,5)} = \frac{1}{4}\int_{-1}^{1}\int_{-1}^{1}\tilde{u}_i(\zeta,\eta=\mp1,\xi)d\zeta d\xi = W_{i(000)} \mp W_{i(010)} + W_{i(020)}$$

$$\langle\tilde{u}_i\rangle^{(4,6)} = \frac{1}{4}\int_{-1}^{1}\int_{-1}^{1}\tilde{u}_i(\zeta=\pm1,\eta,\xi)d\eta d\xi = W_{i(000)} \pm W_{i(100)} + W_{i(200)} \tag{14}$$

Solving for the first and second order coefficients in terms of the fluctuating surface-averaged displacements and the zeroth order coefficients,

$$\begin{Bmatrix} W_{i(100)} \\ W_{i(010)} \\ W_{i(001)} \\ W_{i(200)} \\ W_{i(020)} \\ W_{i(002)} \end{Bmatrix} = \frac{1}{2}\begin{bmatrix} 0 & 0 & 0 & 1 & 0 & -1 \\ 0 & 0 & -1 & 0 & 1 & 0 \\ -1 & 1 & 0 & 0 & 0 & 0 \\ 0 & 0 & 0 & 1 & 0 & 1 \\ 0 & 0 & 1 & 0 & 1 & 0 \\ 1 & 1 & 0 & 0 & 0 & 0 \end{bmatrix}\begin{Bmatrix} \langle\tilde{u}_i\rangle^{(1)} - W_{i(000)} \\ \langle\tilde{u}_i\rangle^{(2)} - W_{i(000)} \\ \langle\tilde{u}_i\rangle^{(3)} - W_{i(000)} \\ \langle\tilde{u}_i\rangle^{(4)} - W_{i(000)} \\ \langle\tilde{u}_i\rangle^{(5)} - W_{i(000)} \\ \langle\tilde{u}_i\rangle^{(6)} - W_{i(000)} \end{Bmatrix} \tag{15}$$

Denoting by C_{ij} and G_{ij} the components of the elastic stiffness matrix of the material, respectively, the local equilibrium equations (6) can be written as

$$C_{11}\frac{\partial^2\tilde{u}_1}{\partial y_1^2} + G_{12}\frac{\partial^2\tilde{u}_1}{\partial y_2^2} + G_{31}\frac{\partial^2\tilde{u}_1}{\partial y_3^2} + (C_{12}+G_{12})\frac{\partial^2\tilde{u}_2}{\partial y_1\partial y_2} + (C_{13}+G_{31})\frac{\partial^2\tilde{u}_3}{\partial y_1\partial y_3} = 0$$

$$G_{12}\frac{\partial^2\tilde{u}_2}{\partial y_1^2} + C_{22}\frac{\partial^2\tilde{u}_2}{\partial y_2^2} + G_{23}\frac{\partial^2\tilde{u}_2}{\partial y_3^2} + (C_{12}+G_{12})\frac{\partial^2\tilde{u}_1}{\partial y_1\partial y_2} + (C_{23}+G_{23})\frac{\partial^2\tilde{u}_3}{\partial y_2\partial y_3} = 0$$

$$G_{31}\frac{\partial^2\tilde{u}_3}{\partial y_1^2} + G_{23}\frac{\partial^2\tilde{u}_3}{\partial y_2^2} + C_{33}\frac{\partial^2\tilde{u}_3}{\partial y_3^2} + (C_{13}+G_{31})\frac{\partial^2\tilde{u}_1}{\partial y_1\partial y_3} + (C_{23}+G_{23})\frac{\partial^2\tilde{u}_2}{\partial y_2\partial y_3} = 0 \tag{16}$$

From equations (5), (15) and (16), the first and second order coefficients can be related to the surface averaged fluctuating displacements by

$$\begin{Bmatrix} \boldsymbol{W}_1 \\ \boldsymbol{W}_2 \\ \boldsymbol{W}_3 \end{Bmatrix} = \bar{\boldsymbol{B}}\begin{Bmatrix} \langle\tilde{\boldsymbol{u}}\rangle^{(1)} \\ \langle\tilde{\boldsymbol{u}}\rangle^{(2)} \\ \langle\tilde{\boldsymbol{u}}\rangle^{(3)} \\ \langle\tilde{\boldsymbol{u}}\rangle^{(4)} \\ \langle\tilde{\boldsymbol{u}}\rangle^{(5)} \\ \langle\tilde{\boldsymbol{u}}\rangle^{(6)} \end{Bmatrix} \tag{17}$$

where $\boldsymbol{W}_i = [W_{i(100)} \quad W_{i(010)} \quad W_{i(001)} \quad W_{i(200)} \quad W_{i(020)} \quad W_{i(002)}]^t$, $\langle\tilde{\boldsymbol{u}}\rangle^{(i)} = \left[\langle\tilde{u}_1\rangle^{(i)} \ \langle\tilde{u}_2\rangle^{(i)} \ \langle\tilde{u}_3\rangle^{(i)}\right]^t$ and the matrix $\bar{\boldsymbol{B}}$ is obtained in function of the material elastic stiffness constants and inverse of the volume-averaged Jacobian matrix $\bar{\boldsymbol{J}}$. Here, the superscript t indicates transpose vector or matrix.

Introducing (5) and (10) into (9), the vector of surface-averaged strain components for the face p of the subvolume can be written in the form

$$\begin{bmatrix}\langle\varepsilon_{11}\rangle\\ \langle\varepsilon_{22}\rangle\\ \langle\varepsilon_{33}\rangle\\ \langle\gamma_{23}\rangle\\ \langle\gamma_{31}\rangle\\ \langle\gamma_{12}\rangle\end{bmatrix}^{(p)} = \begin{bmatrix}\bar{\varepsilon}_{11}\\ \bar{\varepsilon}_{22}\\ \bar{\varepsilon}_{33}\\ \bar{\gamma}_{23}\\ \bar{\gamma}_{31}\\ \bar{\gamma}_{12}\end{bmatrix} + \overline{\boldsymbol{E}}\begin{bmatrix}\bar{\boldsymbol{J}} & \boldsymbol{0} & \boldsymbol{0}\\ \boldsymbol{0} & \bar{\boldsymbol{J}} & \boldsymbol{0}\\ \boldsymbol{0} & \boldsymbol{0} & \bar{\boldsymbol{J}}\end{bmatrix}\begin{bmatrix}\boldsymbol{A}^{(p)} & \boldsymbol{0} & \boldsymbol{0}\\ \boldsymbol{0} & \boldsymbol{A}^{(p)} & \boldsymbol{0}\\ \boldsymbol{0} & \boldsymbol{0} & \boldsymbol{A}^{(p)}\end{bmatrix}\begin{bmatrix}\boldsymbol{W}_1\\ \boldsymbol{W}_2\\ \boldsymbol{W}_3\end{bmatrix} \tag{18}$$

being

$$\overline{\boldsymbol{E}} = \begin{bmatrix}1&0&0&0&0&0&0&0&0\\ 0&0&0&0&1&0&0&0&0\\ 0&0&0&0&0&0&0&0&1\\ 0&0&0&0&0&1&0&1&0\\ 0&0&1&0&0&0&1&0&0\\ 0&1&0&1&0&0&0&0&0\end{bmatrix} \qquad \boldsymbol{A}^{(1,2)} = \begin{bmatrix}1&0&0&0&0&0\\ 0&1&0&0&0&0\\ 0&0&1&0&0&\mp 3\end{bmatrix}$$

$$\boldsymbol{A}^{(3,5)} = \begin{bmatrix}1&0&0&0&0&0\\ 0&1&0&0&\mp 3&0\\ 0&0&1&0&0&0\end{bmatrix} \qquad \boldsymbol{A}^{(4,6)} = \begin{bmatrix}1&0&0&\pm 3&0&0\\ 0&1&0&0&0&0\\ 0&0&1&0&0&0\end{bmatrix}$$

Using the Cauchy's law, the surface-averaged traction components are given in function of the surface-averaged stresses by

$$\begin{bmatrix}\langle t_1\rangle\\ \langle t_2\rangle\\ \langle t_3\rangle\end{bmatrix}^{(p)} = \begin{bmatrix}n_1&0&0&0&n_3&n_2\\ 0&n_2&0&n_3&0&n_1\\ 0&0&n_3&n_2&n_1&0\end{bmatrix}^{(p)}\begin{bmatrix}\langle\sigma_{11}\rangle\\ \langle\sigma_{22}\rangle\\ \langle\sigma_{33}\rangle\\ \langle\sigma_{23}\rangle\\ \langle\sigma_{31}\rangle\\ \langle\sigma_{12}\rangle\end{bmatrix}^{(p)} \tag{19}$$

where n_1, n_2 and n_3 represent the components of the outward unit vector normal to the subvolume face p.

Considering (7) and (18), the surface-averaged stresses can be expressed by

$$\begin{bmatrix}\langle\sigma_{11}\rangle\\ \langle\sigma_{22}\rangle\\ \langle\sigma_{33}\rangle\\ \langle\sigma_{23}\rangle\\ \langle\sigma_{31}\rangle\\ \langle\sigma_{12}\rangle\end{bmatrix}^{(p)} = \boldsymbol{C}\begin{bmatrix}\bar{\varepsilon}_{11}\\ \bar{\varepsilon}_{22}\\ \bar{\varepsilon}_{33}\\ \bar{\gamma}_{23}\\ \bar{\gamma}_{31}\\ \bar{\gamma}_{12}\end{bmatrix} + \boldsymbol{C}\overline{\boldsymbol{E}}\begin{bmatrix}\langle\bar{\boldsymbol{J}}\rangle & \boldsymbol{0} & \boldsymbol{0}\\ \boldsymbol{0} & \langle\bar{\boldsymbol{J}}\rangle & \boldsymbol{0}\\ \boldsymbol{0} & \boldsymbol{0} & \langle\bar{\boldsymbol{J}}\rangle\end{bmatrix}\begin{bmatrix}\boldsymbol{A}^{(p)} & \boldsymbol{0} & \boldsymbol{0}\\ \boldsymbol{0} & \boldsymbol{A}^{(p)} & \boldsymbol{0}\\ \boldsymbol{0} & \boldsymbol{0} & \boldsymbol{A}^{(p)}\end{bmatrix}\begin{bmatrix}\boldsymbol{W}_1\\ \boldsymbol{W}_2\\ \boldsymbol{W}_3\end{bmatrix} - \begin{bmatrix}\langle\sigma_{11}^{\mathrm{th}}\rangle\\ \langle\sigma_{22}^{\mathrm{th}}\rangle\\ \langle\sigma_{33}^{\mathrm{th}}\rangle\\ 0\\ 0\\ 0\end{bmatrix}^{(p)} \tag{20}$$

being $\boldsymbol{C}$ the stifness matrix of the subvolume material. Substituting (20) into (19) and using (17), the vector of the surface-averaged tractions on the subvolume faces is given in the form

$$\langle\boldsymbol{t}\rangle = \boldsymbol{N}\boldsymbol{C}\bar{\boldsymbol{\varepsilon}} + \boldsymbol{K}\langle\tilde{\boldsymbol{u}}\rangle - \boldsymbol{N}\langle\boldsymbol{\sigma}^{\mathrm{th}}\rangle \tag{21}$$

where $\boldsymbol{K}$ represents the subvolume stiffness matrix, $\bar{\boldsymbol{\varepsilon}} = [\bar{\varepsilon}_{11} \quad \bar{\varepsilon}_{22} \quad \bar{\varepsilon}_{33} \quad \bar{\gamma}_{23} \quad \bar{\gamma}_{31} \quad \bar{\gamma}_{12}]^t$ and

$$\langle\boldsymbol{t}\rangle = \left[\langle\boldsymbol{t}\rangle^{(1)} \ \langle\boldsymbol{t}\rangle^{(2)} \ \langle\boldsymbol{t}\rangle^{(3)} \ \langle\boldsymbol{t}\rangle^{(4)} \ \langle\boldsymbol{t}\rangle^{(5)} \ \langle\boldsymbol{t}\rangle^{(6)}\right]^t \tag{22}$$

$$\boldsymbol{N} = [\boldsymbol{n}^{(1)} \quad \boldsymbol{n}^{(2)} \quad \boldsymbol{n}^{(3)} \quad \boldsymbol{n}^{(4)} \quad \boldsymbol{n}^{(5)} \quad \boldsymbol{n}^{(6)}]^t \tag{23}$$

$$\langle\boldsymbol{\sigma}^{\mathrm{th}}\rangle = \left[\langle\sigma_{11}^{\mathrm{th}}\rangle \quad \langle\sigma_{22}^{\mathrm{th}}\rangle \quad \langle\sigma_{33}^{\mathrm{th}}\rangle \quad 0 \quad 0 \quad 0\right]^t \tag{24}$$

$$\langle\tilde{\boldsymbol{u}}\rangle = \left[\langle\tilde{\boldsymbol{u}}\rangle^{(1)} \ \langle\tilde{\boldsymbol{u}}\rangle^{(2)} \ \langle\tilde{\boldsymbol{u}}\rangle^{(3)} \ \langle\tilde{\boldsymbol{u}}\rangle^{(4)} \ \langle\tilde{\boldsymbol{u}}\rangle^{(5)} \ \langle\tilde{\boldsymbol{u}}\rangle^{(6)}\right]^t \tag{25}$$

being $\boldsymbol{n}^{(p)} = [n_1 \quad n_2 \quad n_3]^{(p)}$. More details about the matrix $\boldsymbol{K}$ can be seen in [18,19].

3.3 Stiffness global of the unit cell

Assembly of the global stiffness matrix is carried out by applying traction and displacement continuity conditions at the common interfaces between adjacent subvolumes of the repeating unit cell. The traction continuity conditions are imposed by applying force balance equations, which are then expressed in terms of the surface-averaged interfacial displacements using the local stiffness matrix equations. The displacement continuity conditions are directly enforced by setting the interfacial surface-averaged displacements to common values. The resulting systems of equations has the following form

$$\boldsymbol{K}^G\langle\widetilde{\boldsymbol{U}}\rangle = \Delta\boldsymbol{C}\bar{\boldsymbol{\varepsilon}} + \Delta\boldsymbol{\Gamma}\Delta T \tag{26}$$

where $\boldsymbol{K}^G$ is the global stiffness matrix of the RUC, $\Delta\boldsymbol{C}$ is a matrix comprised of the differences in the local stiffness matrices of adjacent subvolumes and the matrix $\Delta\boldsymbol{\Gamma}$ involves the thermal contributions.

3.4 Homogenized thermoelastic constitutive relations

The solution of the system (26) provides the global fluctuating surface-averaged displacement vector $\langle\widetilde{\boldsymbol{U}}\rangle$, which allows the computation of the surface-averaged strains $\bar{\boldsymbol{\varepsilon}}^{(k)}$ and, consequently, the elements of the Hill's concentration strain matrix of each subvolume k, using the localization relation

$$\bar{\boldsymbol{\varepsilon}}^{(k)} = \boldsymbol{A}^{(k)}\bar{\boldsymbol{\varepsilon}} \tag{27}$$

Each column of the matrix $\boldsymbol{A}^{(k)}$is generated applying an elementary nonzero macroscopic strain vector $\bar{\boldsymbol{\varepsilon}}$ at a time and solving the system **(**26**)** to obtain the corresponding $\bar{\boldsymbol{\varepsilon}}^{(k)}$by (27).

The macroscopic stress vector $\langle\boldsymbol{\sigma}\rangle$ can be written in function of the corresponding macroscopic strain vector by the overall constitutive equation of the composite

$$\langle\boldsymbol{\sigma}\rangle = \boldsymbol{C}^*\langle\boldsymbol{\varepsilon}\rangle - \boldsymbol{\Gamma}^*\Delta T \tag{28}$$

where the material effective stiffness matrix $\boldsymbol{C}^*$ is obtained by

$$\boldsymbol{C}^* = \sum_{k=1}^{N_k} v^{(k)}\boldsymbol{C}^{(k)}\boldsymbol{A}^{(k)} \tag{29}$$

and $\boldsymbol{\Gamma}^* = \boldsymbol{C}^*\boldsymbol{\alpha}^*$ is given by the Levin's formula [20]

$$\boldsymbol{\Gamma}^* = \sum_{k=1}^{N_k} v^{(k)}\left[\boldsymbol{A}^{(k)}\right]^{\mathrm{t}}\boldsymbol{\Gamma}^{(k)} \tag{30}$$

being $v^{(k)}$ the volume fraction of the subvolume k.

4 Numerical examples

4.1 Effective thermal expansion coefficients of a unidirectional long fiber two-phase composite

Here, the presented model is applied to evaluate thermal expansion coefficients of a periodic composite reinforced by unidirectional long fiber distributed in square arrays. The composite is constituted by an epoxy matrix reinforced with glass fibers. The thermoelastic properties of these constituent materials are presented in Table 1.

The results obtained for the variation of the effective longitudinal and transverse thermal expansion coefficients (α_L, α_T) in function of the fiber volume fraction are shown in Figures 3 and 4, respectively. Here, α_m represents the thermal expansion coefficient of the matrix. For comparison, these figures also present the predictions of a micromechanical model based on the finite-element

method found in Karadeniz and Kumlutas [21]. As observed, the results of the present model (FVT) are in an excellent agreement with those corresponding to the finite-element micromechanical model (FEM).

Table 1. Thermoelastic properties of epoxy matrix and glass fiber

Constituent	$E\ (GPa)$	$G\ (GPa)$	ν	$\alpha\ (/^oC)$
Epoxy	3.5	3.89	0.35	$5.25\text{x}10^{-5}$
Glass	72	40	0.20	$5.00\text{x}10^{-6}$

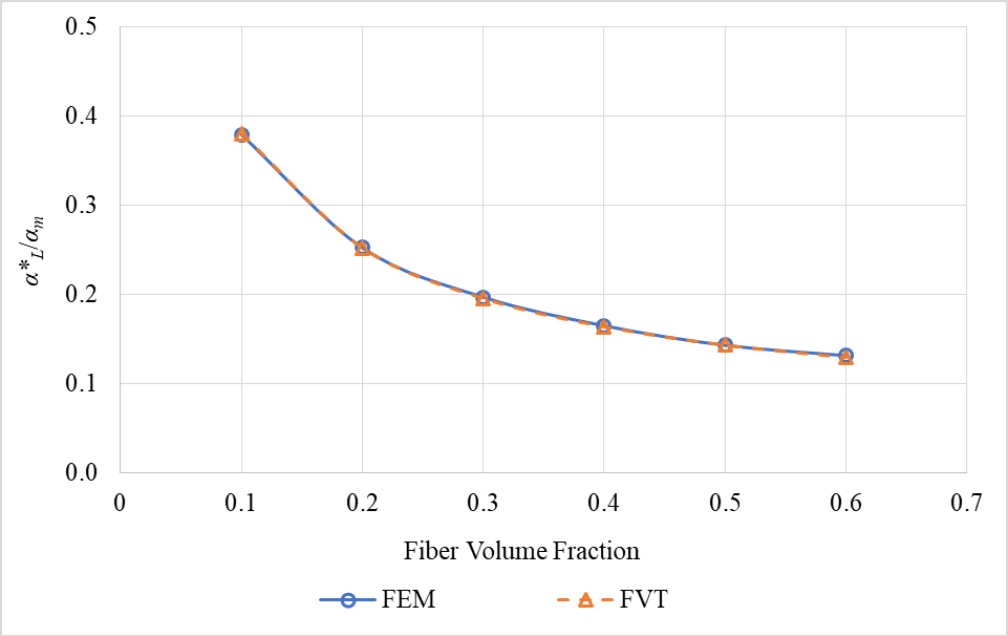

Figure 3. Longitudinal effective thermal expansion coefficient

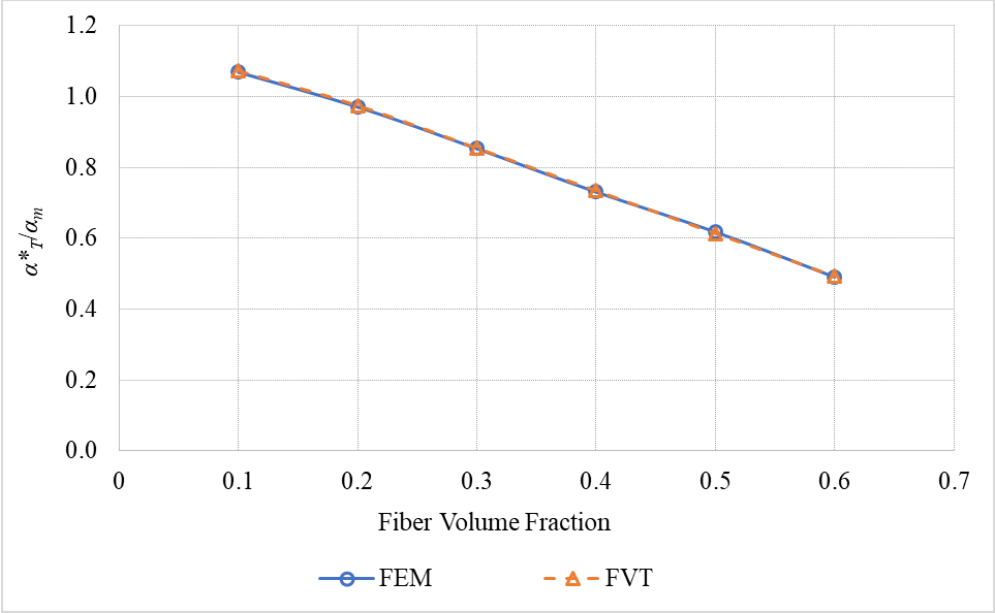

Figure 4. Transverse effective thermal expansion coefficient

4.2 Effective thermoelastic properties of a periodic three-phase composite

This example consists in a unidirectional three-phase composite composed by an aluminium matrix reinforced by SiC cylindrical fibers coated with a thin carbon interphase. The thermoelastic properties of the constituent materials are presented in Table 2. The fibers are periodically distributed in a square array with a volume fraction of 40%. The thickness of the interphase is $0.13\ \mu m$ and the fibers have a diameter of $20\ \mu m$.

Table 2. Thermoelastic properties of the constituent materials

Constituent	$E\ (GPa$	$G\ (GPa)$	ν	α (/°C)
Aluminium matrix	96.5	37.1	0.3	$9.25\text{x}10^{-6}$
SiC fiber	431	172	0.25	$4.86\text{x}10^{-6}$
Carbon interphase	34.48	14.34	0.20	$3.30\text{x}10^{-6}$

Table 3 shows the results of the effective thermoelastic properties provided by the FVT model for two cases: composite without interphase and composite with interphase. Analytical predictions obtained by Dasguptha and Bhandarkar [22], using a generalized self-consistent Mori-Tanaka scheme, are also presented in Table 3. The axis 1 coincides with the fiber direction while the axes 2 and 3 are in the transverse directions. As can be observed, the numerical and analytical solutions, in general, present a very good approximation.

Table 3. Effective thermoelastic properties

Effective properties	Without interphase		With interphase	
	FVT	Analytical	FVT	Analytical
$\boldsymbol{E_1^*}$(GPa)	230,24	230,37	229,52	229,71
$\boldsymbol{G_{12}^*}$ (GPa)	63,06	62,91	61,54	61,39
$\boldsymbol{G_{23}^*}$ (GPa)	56,36	59,57	55,20	57,99
$\boldsymbol{\alpha_L^*}$ (/°C)	$6\text{x}10^{-6}$	$5{,}99\text{x}10^{-6}$	$5{,}99\text{x}10^{-6}$	$5{,}98\text{x}10^{-6}$
$\boldsymbol{\alpha_T^*}$ (/°C)	$7{,}64\text{x}10^{-6}$	$7{,}64\text{x}10^{-6}$	$8{,}25\text{x}10^{-6}$	$7{,}60\text{x}10^{-6}$

4.3 Unidirectional short fiber periodic composite materials

This example considers a periodic unidirectional composite composed by an aluminium matrix reinforced by aligned SiC short cylindrical fibers with the elastic properties shown in Table 2. The fibers have a length L and cross section radius r. The objective is to analyze the influence of the aspect ratio of the fiber ($\rho = L/2r$) on the effective elastic moduli of the material. The microstructure of the composite is defined by a cuboidal repeating unit cell with square cross section normal to the fiber direction of side a and length $b = 2.5\ a$. It is assumed a fiber volume fraction $v_f = 0.30$. The maximum and minimum fiber aspect ratios are given by $\rho_{max} = 0.5(b/a)\sqrt{\pi/v_f}$ and $\rho_{min} = 4v_f b/(\pi a)$, respectively. Then, for the particular values adopted in this example, the extreme fiber aspect ratios are $\rho_{max} \cong 4.04$ and $\rho_{min} \cong 0.95$.

The results provided by the model for the variations of the effective elastic properties in function of the fiber aspect ratio ($1.3 \leq \rho \leq 3.8$) are presented in Figures 5-7. Figure 5 illustrates the variation of the effective Young's moduli for the fiber direction (1) and transverse direction (2). It is observed that when ρ increases the values of E_1^* increase while those of E_2^* decrease. This behavior occurs because a rise of ρ is associated with increase of L and reduction of r because v_f must keep constant and, consequently, the longitudinal stiffness increases and the transverse stiffness decreases. Figures 6 and 7 show the variation of effective shear moduli and Poisson's ratios for the longitudinal plane (1-2) and transverse plane (2-3) in function of the fiber aspect ratio, respectively. It is observed that the effective shear modulus in the plane 1-2, G_{12}^*, has a small dependency of the fiber aspect ratio. The

transverse effective shear modulus G_{23}^{*} is reduced when ρ increases because the fiber radius must decrease to keep constant the fiber volume fraction. A similar explanation can be used to justify the increase of the effective Poisson's ratios for increasing fiber aspect ratio shown in Fig. 7.

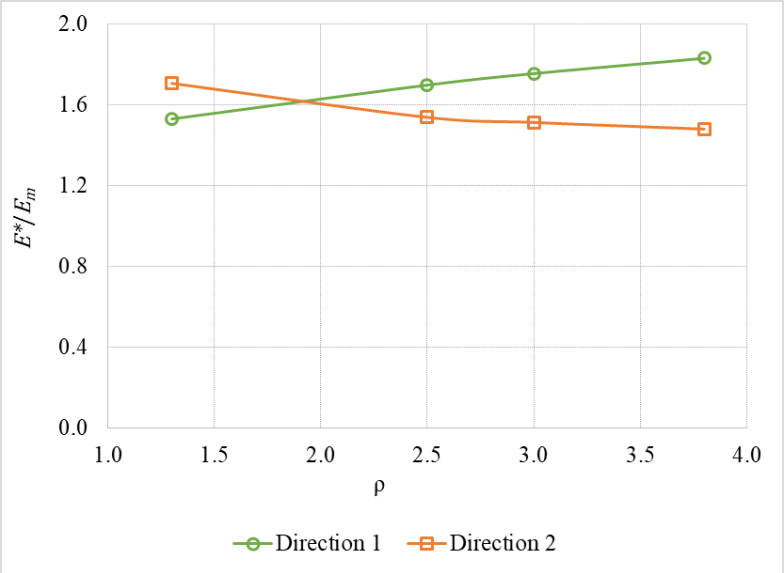

Figure 5. Longitudinal and transverse effective Young's moduli

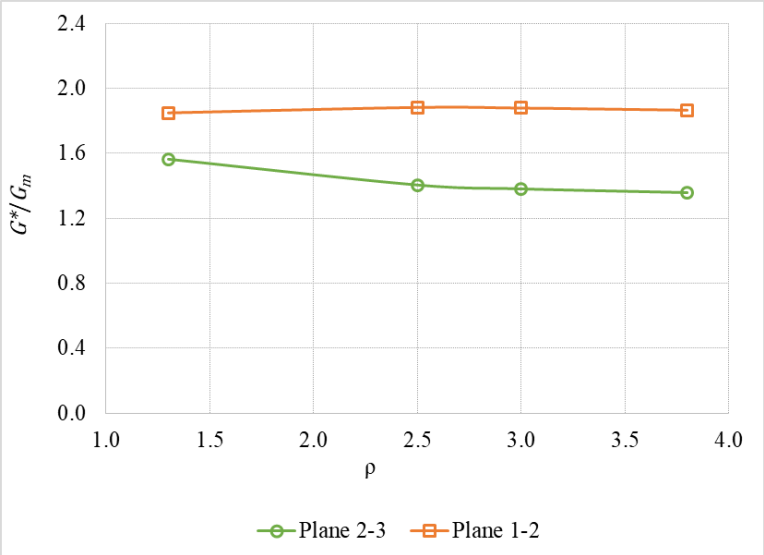

Figure 6. Effective longitudinal and transverse shear moduli

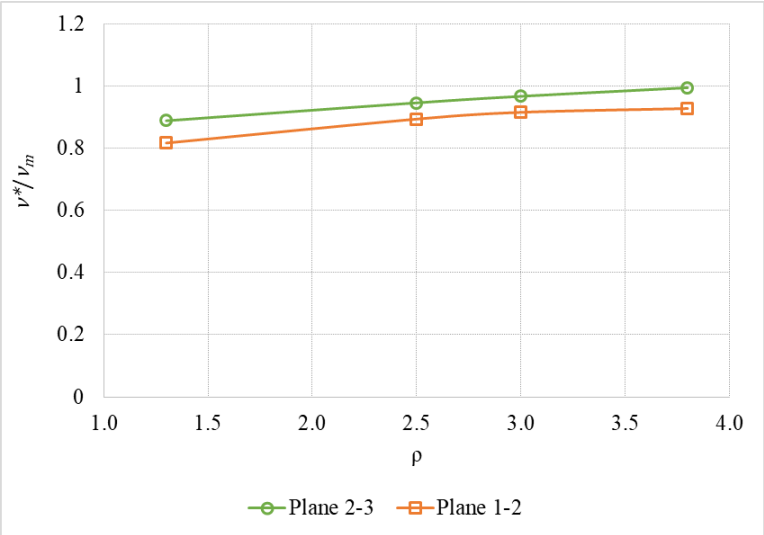

Figure 7. Effective Poisson's ratios in the longitudinal and transverse planes

5 Conclusions

This work presented a theoretical study on the evaluation of the effective thermoelastic properties de composites with periodic microstructures using a three-dimensional micromechanical model based on the parametric finite-volume formulation. The model has been applied to evaluate the elastic moduli and thermal expansion coefficients of unidirectional periodic composites reinforced by continuous and short fibers. The performance of the model has been verified through comparisons of its results with analytical and finite-element solutions.

Acknowledgements

The authors acknowledge the financial support provided by the Brazilian agencies CNPq, FAPEAL and CAPES.

References

[1] S. Nemat-Nasser and M. Hori. *Micromechanics: Overall properties of heterogeneous materials, second ed., Elsevier Science Publishers*, Amsterdam, 1999.
[2] M. A. A. Cavalcante, M. - J. Pindera and H. Khatam, Finite-volume micromechanics of periodic materials: past, present and future, *Composites Part B*, vol. 43, n. 6, pp. 2521-2543, 2012.
[3] J. D. Eshelby. The determination of the elastic field of an ellipsoidal inclusion, and related problems. *Proceedings of the Royal Society A*, vol. 241, pp. 376–396, 1957.
[4] R. Hill. Theory of mechanical properties of fibre-strengthened materials - III. Self-consistent model, *Journal of the Mechanics and Physics of Solids*, vol. 13, pp. 189-198, 1965.
[5] T. Mori and K. Tanaka. Average stress in matrix and average elastic energy of materials with misfitting inclusions. *Acta Metallurgica*, vol. 21, pp. 571–574, 1973.
[6] Y. Benveniste. New approach to the application of Mori-Tanaka's theory. *Mechanics of Materials*, vol.6, pp. 147–157, 1987.
[7] R. McLaughlin. A study of the differential scheme for composite materials. *International Journal of Engineering Science*, vol. 15, pp. 237-244, 1977.
[8] A. N. Norris. A differential scheme for the effective moduli of composites. *Mechanics of Materials*, vol. 4, pp. 1-16, 1985.

[9] H. Hatta and M. Taya. Equivalent inclusion method for steady state heat conduction in composites. *International Journal of Engineering Science*, vol. 24, n. 7, pp. 1159–1172, 1986.
[10] P. Lu, Further studies on Mori-Tanaka models for thermal expansion coefficients of composites. *Polymer,* vol. 54, pp. 1691-1699, 2013.
[11] J. C. Michel, H. Moulinec and P. Suquet. Effective properties of composite materials with periodic microstructure: a computational approach. *Computer Methods in Applied Mechanics and Engineering*, vol. 172, n. 1, pp. 109‑143, 1999.
[12] V. I. Kushch and I. Sevostianov. Effective elastic properties of the particulate composite with transversely isotropic phases. *International Journal of Solids and Structures,* vol. 41, n. 3-4, pp. 885-906, 2004.
[13] K. Liu, H. Takagi, R. Osugi and Z. Yang. Effect of physicochemical structure of natural fiber on transverse thermal conductivity of unidirectional abaca/bamboo fiber composites. *Composites Part A*, vol. 43, n. 8, pp. 1234–1241, 2012.
[14] M. Gattu, H. Khatam, A. S. Drago and M.- J. Pindera. Parametric finite-volume micromechanics of uniaxial, continuously-reinforced periodic materials with elastic phases. *Journal of Engineering Materials and Technology*, vol. 130, n. 3, 031015-15, 2008.
[15] Luciano R, Barbero EJ (1994) Formulas for the stiffness of composites with periodic microstructure. Int J Solids Struct 31(21):2933-2944.
[16] E. N. Lages and S. P. C. Marques. A semi-analytical model for evaluation of effective thermal conductivity of composites with periodic microstructure. *Journal of the Brazilian Society of Mechanical Sciences and Engineering*, vol. 41:127, 2019.
[17] Q. Chen, X. Chen, Z. Zhai and Z. Yang. A new and general formulation of three-dimensional finite-volume micromechanics for particulate reinforced composites with viscoplastic phases. *Composite Part B*, v. 85, pp. 216-232, 2016.
[18] Q. Chen, G. Wang and X. Chen. Three-dimensional parametric finite-volume homogenization of periodic materials with multi-scale structural applications. *International Journal of Applied Mechanics*, v. 10, n. 4, 1850045, 2018.
[19] C. S. Vieira. Thermal and elastic homogenization of periodic composites with interphases. PhD thesis, Federal University of Alagoas, 2018.
[20] V. M. Levin, On the coefficients of thermal expansion of heterogeneous materials. *Mechanics of Solids*, vol. 2, pp. 58-61, 1967.
[21] Z. H. Karadeniz and D. Kumlutas. A numerical study on the coefficients of thermal expansion of fiber reinforced composite materials. *Composite Structures*, vol. 78, n. 1, pp. 1-10, 2007.
[22] A. Dasgupta and S. M. Bhandarkar. A generalized self-consistent mori-tanaka scheme for fiber-composites with multiple interphases. *Mechanics of Materials*, vol. 14, n. 1, pp. 67-82, 1992.